THE JOURNAL OF PHYSICAL CHEMISTRY C

Article

pubs.acs.org/JPCC

Experimental and First-Principles Theoretical Study of Structural and Electronic Properties in Tantalum-Doped In_2O_3 Semiconductor: Finding a Definitive Hyperfine Interaction Assignment

Diego Richard,*[,†,‡] Germán N. Darriba,[†,‡] Emiliano L. Muñoz,[‡] Leonardo A. Errico,[†,‡,§] Paul D. Eversheim,[∥] and Mario Rentería[†,‡]

[†]Departamento de Física, Facultad de Ciencias Exactas, Universidad Nacional de La Plata, CC 67, (1900) La Plata, Argentina

[‡]Instituto de Física La Plata (IFLP, CCT-La Plata, CONICET-UNLP), Facultad de Ciencias Exactas, Universidad Nacional de La Plata, CC 67, (1900) La Plata, Argentina

[§]Universidad del Noroeste de la Provincia de Buenos Aires (UNNOBA), Monteagudo 2772, (2700) Pergamino, Argentina

[∥]Helmholtz-Institut für Strahlen-und Kernphysik (H-ISKP), Universität Bonn, Nussallee 14−16, 53115 Bonn, Germany

Supporting Information

ABSTRACT: In this work we present an experimental and theoretical study from first-principles of the structural, electronic, and hyperfine properties of Ta-doped In_2O_3 semiconductor. The *ab initio* electronic structure calculations in the Ta-diluted In_2O_3 system enabled to obtain the structural lattice distortions and the hyperfine parameters when the Ta atom is placed at each cationic site of the *bixbyite* crystal structure. To this purpose we used the full-potential augmented plane wave plus local orbital (FP-APW+lo) method, within the density functional theory. The obtained results indicate that the substitutional Ta probe-impurity produces strong changes on the local structure. In addition, we performed accurate time-differential perturbed $\gamma-\gamma$ angular correlations (TDPAC) key experiments in $^{181}Hf(\rightarrow{}^{181}Ta)$-implanted In_2O_3 samples with high crystallinity, in order to obtain high quality measurements of the electric-field gradient tensor (EFG) that unraveled the controversy settled in the literature and overcome dissimilar interpretations of previously reported TDPAC experiments. The experiments were performed at room temperature in air, after each step of a series of thermal annealing treatments in air at increasing temperatures in order to remove radiation damage and locate the ^{181}Hf probes at substitutional cationic sites. We succeeded to obtained two well-defined hyperfine interactions that were assigned to ^{181}Ta probes located at the two defect-free inequivalent cationic sites of the In_2O_3 crystal structure. The EFG calculations are in excellent agreement with the results of these TDPAC measurements, and show that the largest component of the diagonalized EFG, V_{33}, at the Ta site has mainly *p* character. The accuracy of the experiments together with the reliable and precise *ab initio* results allowed a definitive determination of the EFG at both cationic sites in this system. Formation energy calculations of defects were needed to determine the charge state of the ^{181}Ta impurity, which agrees with a semiconducting character for the In_2O_3:Ta doped system.

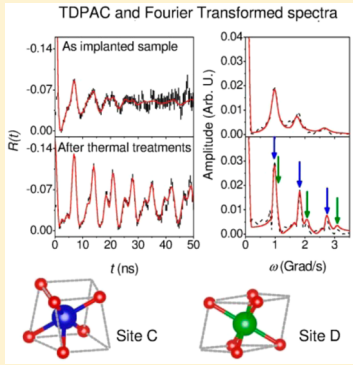

I. INTRODUCTION

Indium oxide (In_2O_3) is a transparent conducting oxide (TCO) that crystallizes in the *bixbyite* structure. It has gained current technological interest due to its potential applications in microelectronics,[1,2] solar cells,[3,4] and sensors,[5,6] among other promising technological new fields like, e.g., in spintronics.[7−10]

Different hyperfine techniques has been employed in the study of pure[11] and doped In_2O_3. Particularly, the time-differential perturbed $\gamma-\gamma$ angular correlation (TDPAC) technique have been systematically applied to the study of hyperfine interactions in a very wide group of binary oxides,[12] being In_2O_3 the first oxide studied with $(^{111}In \rightarrow)^{111}Cd$ impurity probe-atoms.[13−17] This technique could give very accurate information about the subnanoscopic environment around a probe nucleus through the determination of the electric-field gradient tensor (EFG) at this site. In this respect, the EFG is a very sensitive observable, which originates from the nonspherical charge distribution surrounding the probe nucleus. It is defined as the second derivate, with respect to the spatial coordinates, of the Coulomb potential $V(\vec{r})$ of these surrounding charges around the probe nucleus.

More recently, different first-principles methods have been used to study theoretically pure and doped In_2O_3.[18−24] The development of certain methods for electron-density calculation in solids in the framework of density functional theory (DFT) opened the possibility to study the EFG in pure and doped binary oxides, combining hyperfine techniques results and first-principles calculations.[25−36] This kind of calculations

Received: November 13, 2015
Revised: February 5, 2016
Published: February 8, 2016

DOI: 10.1021/acs.jpcc.5b11155
J. Phys. Chem. C 2016, 120, 5640−5650

provides a realistic model for an accurate description of subtle details of the electronic structure also very close to the nucleus, and therefore of the EFG, which reproduces accurately the experimental value, and also provides information about the physics behind it and its origin. The goal of these experimental and theoretical approaches is to determine the arising physical properties that are induced by the presence of the impurities.

Employing this combined experimental and theoretical approach many Cd-doped *bixbyite* oxides, and in particular In_2O_3, where studied.[34,37−39] On the other hand, the study of Ta-doped *bixbyites* using this approach is at an initial stage, and only the Sc_2O_3:Ta system has been analyzed.[40]

Concerning ^{181}Ta-doped In_2O_3, previous TDPAC studies of the EFG at the probe site where reported by Vercesi et al.[41] and Rentería et al.[42] Both experiments gave dissimilar results. The assignment of the hyperfine interactions associated with ^{181}Ta probes located at the both substitutional C and D cationic sites, in both experiments, was based in very simple models available at that time. At this point, the puzzling issue is how to explain these significant differences between previous experiments, and to know which are the hyperfine interaction associated with Ta probes located at cationic sites C and D.

In order to solve the controversies related with the assignment of the hyperfine interactions at ^{181}Ta sites in In_2O_3 reported in previous experiments of the literature, we have performed an *ab initio* DFT study that gives a complete description of structural and electronic effects introduced by the impurity in this oxide semiconductor, without the use of external parameters. In addition, in order to confirm our theoretical predictions and to give a definite hyperfine characterization at ^{181}Ta impurities at substitutional cationic sites we performed careful and high-statistic key TDPAC experiments in ^{181}Hf-implanted In_2O_3 samples with a high degree of crystalinity.

In what follows, in section II we present the TDPAC technique and the In_2O_3 crystal *bixbyite* structure. In section III, the first-principles procedure is introduced, and we present and discuss the corresponding theoretical predictions for the electronic and structural properties, and the EFG. In section IV, we present a brief review of the previous experimental results in In_2O_3 using ^{181}Ta, the sample preparation for the key experiment, how measurements were performed, and our experimental results are discussed and confronted with the *ab initio* predictions. In section V, we compare our results with the previous experiments and, finally, in section VI, the conclusions are given.

II. EXPERIMENTAL SECTION

A. The TDPAC Technique. During a nuclear-decay $\gamma-\gamma$ cascade, the extra-nuclear fields (with nonspherical symmetry) can perturbate the angular correlation between the emission of the two successive γ radiations. The TDPAC spectroscopy is based on the experimental determination of these perturbations. In this sense, the hyperfine interaction between the nuclear quadrupole moment Q and an extra-nuclear EFG lead to precession frequencies (ω_n) of the time spectral signal that can be measured by TDPAC and are proportional to V_{33}, the largest component of the diagonalized EFG.[43]

The TDPAC experiments presented in this work were performed using the 133−482 keV $\gamma-\gamma$ cascade of ^{181}Ta, emitted after the β^- nuclear decay of the ^{181}Hf father-isotope. In a typical TDPAC experiment using ^{181}Hf → ^{181}Ta tracers, the goal is to introduce the ^{181}Hf atoms at substitutional cationic sites using different doping methods. The hyperfine interaction occurs at the ^{181}Ta daughter probe-atom, being commonly assumed that the ^{181}Ta atom remains localized at the same crystallographic site occupied by the ^{181}Hf atom before the β^- decay. During the $\gamma-\gamma$ decay, the ^{181}Ta isotope pass through an intermediate nuclear level with spin $I = +^5/_2$, for which Q_{Ta} (482 keV, $I = +^5/_2$) = +2.35(6) b.[44] For polycrystalline samples, functions of the form $A_{22}^{exp}G_{22}(t)$, folded with the time resolution curve of the spectrometer, are usually employed to fit the measured TDPAC spectrum, called $R(t)$. For electric-quadrupole interactions

$$R(t) \approx A_{22}^{exp}G_{22}(t) = A_{22}^{exp}\sum_i f_i\left(S_{20,i} + \sum_{n=1}^{3}\left[S_{2n,i}\cos(\omega_{n,i}t)e^{-\delta_i\omega_{n,i}t}\right]\right) \quad (1)$$

where A_{22}^{exp} is the experimental anisotropy of the $\gamma-\gamma$ cascade, $G_{22}(t)$ is the so-called perturbation factor, and f_i is the relative fraction of nuclei that experience the i-th perturbation. For each contribution to $R(t)$, the ω_n frequencies are related by $\omega_n = g_n(\eta)\nu_Q$ to the quadrupole coupling constant $\nu_{Q=} eQV_{33}/h$. The exponential functions in eq 1 account for Lorentzian frequency distributions of relative width δ around ω_n. The g_n and S_{2n} coefficients are known functions of the asymmetry parameter η.[45] In the principal axis system the largest diagonal component V_{33} and the asymmetry parameter $\eta = (V_{11} - V_{22})/V_{33}$ (using the standard convention $|V_{11}| \le |V_{22}| \le |V_{33}|$) determine completely the EFG, since in this system the EFG is traceless.

The Fourier transformation of the $R(t)$ spectrum shows the ω_n values in the frequency spectrum. For TDPAC probes with $I = {}^5/_2$, each hyperfine interaction results in a triplet of these frequencies in the Fourier transformed spectrum, depending the position of each peak on η and V_{33}.

B. Crystal Structure. In_2O_3 adopts the *bixbyite* structure (body-centered cubic, space group $Ia\bar{3}$), with a lattice parameter a = 10.118 Å at T = 300 K.[46,47] The unit cell contains 32 In and 48 O atoms, and presents two inequivalent crystallographic 24d and 8b sites for cations, called C and D, respectively, both O_6 coordinated (see Figure 1a), with a relative abundance of the C sites over the D sites of 3:1. Site C has a 2-fold symmetry (C_2 point symmetry), while site D is

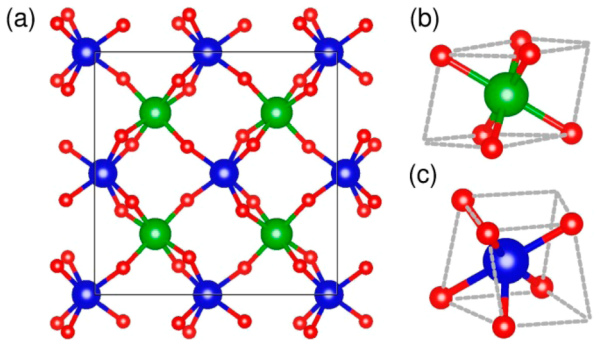

Figure 1. (a) Unit cell layer of the In_2O_3 *bixbyite* structure along the (001) plane. The large green and blue spheres stand for the nonequivalent cationic sites D and C, respectively, and the small red spheres represent oxygen atoms. (b, c) Illustration of the nearest-neighbor oxygen octahedron arrangements around cationic sites D and C (parts b and c, respectively). In each case the oxygen atoms lie at the corners of a distorted cube denoted by dotted lines, with two of its corners unoccupied (see text).

DOI: 10.1021/acs.jpcc.5b11155
J. Phys. Chem. C 2016, 120, 5640−5650

centrosymmetric (C_{3i} point symmetry). The internal positions of the atoms in the unit cell are determined by the u, x, y, and z parameters, where u = 0.4668(1) determines the positions of C-type cations, and x = 0.3905(13), y = 0.1529(11), and z = 0.3832(13) determine those of the oxygen atoms.[47]

Site D can be viewed as a cation surrounded by six oxygen nearest neighbors (ONNs), which lie at the corners of a distorted cube, with two opposite corners on a cube diagonal unoccupied. In this case, each ONN is at the same distance d_{NN}= 2.19 Å from the In atom (Figure 1b). For site C, there are also six ONNs around the In atom, but in this case they lie at the corners of a more distorted cube, belonging the unoccupied corners to a face diagonal of such cube (see Figure 1c). At this site there are three different pairs of bond-lengths with d_{NN} = 2.12, 2.19, and 2.21 Å.

According to the *bixbyite* structure and the geometry of both cationic sites it is expected EFGs with $\eta^C > 0.5$ and $\eta^D = 0$ for probes located at C and D sites, respectively, and with a relative site population of $f^C/f^D = 3$. Additionally, based in a simple geometrical point-charge model it is expected that the V_{33} value associated with probes at the symmetric cationic sites will be twice as large than those of the asymmetric site ($V_{33}{}^D \approx 2V_{33}{}^C$). These characteristics predicted by this simple model are in qualitative agreement with the experimental results observed in many *bixbyite* oxides doped with ^{111}Cd as probe (see refs 34 and 48 and references therein) and also in other ^{181}Ta-doped *bixbyite* sesquioxides with lattice parameter larger than that of In_2O_3.[48] This agreement led to think to some researchers in the 90's that the ^{111}Cd impurity did not introduce structural and electronic distortions in the host lattice[49] and, afterward, similar conclusions were proposed for ^{181}Ta in *bixbyites*.[12]

III. COMPUTATIONAL APPROACH

A. First-Principles Procedure. The DFT-based *ab initio* calculations were performed with the WIEN2k implementation of the Full-Potential Augmented Plane Wave plus local orbital (FP-APW+lo) method.[50] In this method, the wave functions are expanded in terms of spherical harmonics inside non-overlapping atom-centered spheres of radius R_{MT}, and in plane waves in the interstitial region.[51] The R_{MT} were 1 Å for In, Hf, and Ta atoms, and 0.9 Å for O atoms. Integration in the reciprocal space was carried out using the tetrahedron method[52] and taking 100 k-points in the first Brillouin zone. The wave functions in the interstitial region were expanded in planewaves using a cutoff parameter $R_{MT}K_{max}$ = 7, where K_{max} is the maximum modulus of the reciprocal lattice vectors. The exchange and correlation effects were treated using both the local-density approximation (LDA)[53] and the generalized-gradient approximation proposed by Wu and Cohen (WC-GGA).[54] To determine the structural distortions induced by the impurity, when the self-consistency of the potential was achieved, the forces on the atoms were obtained, and they were displaced until the forces on them were below a tolerance value of 0.025 eV/Å, in order to predict the final equilibrium structures.

In order to study the Ta-doped In_2O_3 systems from first-principles, we have to consider first the radioactive father of ^{181}Ta, namely ^{181}Hf, thus making the reasonable assumption that the ^{181}Ta atom remains at the same site selected by the ^{181}Hf atom before the ^{181}Hf → ^{181}Ta β^- decay. In this way, we first considered the unit cell of In_2O_3 in which one In atom of type C or D is replaced by a Hf atom. We call these doped systems In_2O_3:Hf(C) and In_2O_3:Hf(D), respectively. The energy difference between the systems In_2O_3:Hf(C) and In_2O_3:Hf(D) can be used to predict the relative occupation (site preference) of the ^{181}Hf atom (and hence of the daughter ^{181}Ta atom) in the structure. After this, and in order to analyze the doped system with the ^{181}Ta-TDPAC probe-atom, one In atom of type C or D was replaced by a Ta atom in the unit cell, as it was done for the case of the Hf atom. We call these doped systems In_2O_3:Ta(C) and In_2O_3:Ta(D). In all the doped systems used in this work, the impurity cation dilution is 3.125 at. %. As a general scheme of the calculations, we initially fixed the lattice parameter and the internal atomic positions of the atoms at their experimental values, and then we allowed the structure to freely relax, to find the final atomic positions. The lattice parameter and angles of the unit cell were kept fixed at their experimental values during the structural relaxation, since the ppm impurity dilution in the TDPAC samples is extremely high to change the cell volume.

Since the substitutional Ta^{5+} impurity has a nominal double-donor character in $In_2{}^{3+}O_3{}^{2-}$, to simulate the different charge states of the impurity we considered three different cases by removing none (In_2O_3:Ta^0), one (In_2O_3:Ta^{1+}), or two (In_2O_3:Ta^{2+}) electrons from the cell. The same considerations were taking into account for the single-donor character of the Hf^{4+} in $In^{3+}{}_2O^{2-}{}_3$, and therefore we performed calculations by removing none (In_2O_3:Hf^0) or one (In_2O_3:Hf^{1+}) electron from the cell.

To study the EFG at a given atom, in each step of the self-consistent calculation, the V_{ii} principal components of the EFG tensor were determined from the radial coefficients V_{2M} of the lattice harmonic expansion of the potential.[55,56] In this way, we calculated the EFG for the unrelaxed and relaxed structures and the different charge states of the cell.

B. Theoretical Results and Discussion. In order to understand the changes introduced in the electronic structure of In_2O_3 by the Ta impurity, we briefly review the electronic structure of pure In_2O_3. As can be seen in Figure 2a, using

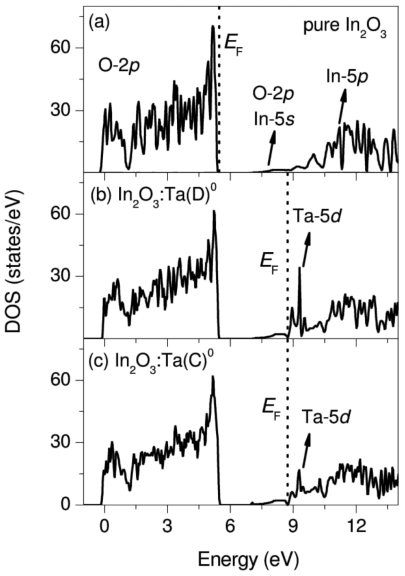

Figure 2. LDA-calculated density of states (DOS) for (a) pure In_2O_3, and (b, c) Ta doping In_2O_3 at site D and C, (In_2O_3:$Ta(D)^0$ and In_2O_3:$Ta(C)^0$, respectively), after structural relaxation. In each figure, the vertical dashed line indicates the Fermi energy E_F.

DOI: 10.1021/acs.jpcc.5b11155
J. Phys. Chem. C 2016, 120, 5640−5650

LDA, the valence band (VB) of this system has predominantly O-2p character, with a smaller contribution of the In orbitals, and the conduction band (CB) is due to In-5s and In-5p states, with an hybridization with O-2p states at the bottom of this band. A detailed description of each atomic contribution to the lower energy region of the CB is shown in Figure 3a. Using

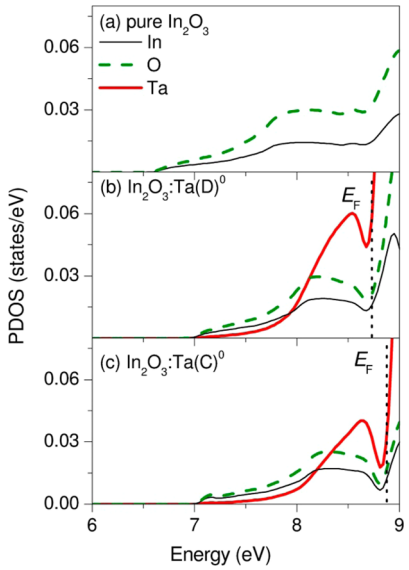

Figure 3. LDA-calculated atom-projected partial density of states (PDOS) near the conduction band minimum for (a) pure In_2O_3, and (b, c) Ta doping In_2O_3 at site D and C (In_2O_3:Ta(D)^0 and In_2O_3:Ta(C)^0, respectively), after structural relaxation. These are contributions of single atomic sphere (for In and O atoms they correspond to a mean contribution per sphere). In parts b and c, the vertical dashed line indicates the Fermi energy E_F.

WC-GGA for the exchange and correlation energy we obtain the same results, being the overall structure of the calculated density of states (DOS) for the pure system consistent with those obtained in other first-principles studies.[18,21−23,37]

As explained in section III.A, the energy difference between In_2O_3:Hf(C) and In_2O_3:Hf(D) systems enable us to predict the preference of the ^{181}Hf-daughter (i.e., ^{181}Ta atom) for each cation site in In_2O_3 structure. We have to remember here that we are based in the reasonable hypothesis that the ^{181}Hf-($\rightarrow^{181}$Ta) β^- decay does not change the lattice sites selected by hafnium. If the same energy is found for the systems In_2O_3:Hf(C) and In_2O_3:Hf(D), a random occupation of the sites is expected ($f^C/f^D = 3$). We found that the energy of the system In_2O_3:Hf(C) is 0.19 eV smaller than that of the system In_2O_3:Hf(D), showing a Hf preference for site C. This result was obtained using LDA in the calculations, the neutral charge state for the Hf impurity (Hf^0, i.e., none electron is removed from the cell), and considering the structural distortions induced by Hf. This energy difference is very similar to that obtained when one electron is removed from the cell, 0.17 eV. These results do not change if WC-GGA is used. This preference should imply a relative ^{181}Ta population $f^C/f^D > 3$, i.e., larger than that expected for a homogeneous Ta distribution among cationic sites C and D. Afterward, since the final equilibrium structures of In_2O_3:Hf(C) and In_2O_3:Hf-(D) for both In_2O_3:Hf^0 and In_2O_3:Hf^{1+} charge states are practically the same, we replaced the Hf atom by a Ta atom at the In_2O_3:Hf(C)^0 and In_2O_3:Hf(D)^0 relaxed structures. At these positions we found an EFG characterized by $V_{33}^C = -19.93 \times 10^{21}$ V/m^2 and $\eta^C = 0.09$ for C site and $V_{33}^D = +13.01 \times 10^{21}$ V/m^2 and $\eta^D = 0$ for D. If we remove 2 electrons we found an EFG characterized by $V_{33}^C = -18.09 \times 10^{21}$ V/m^2 and $\eta^C = 0.21$ for C site and $V_{33}^D = +23.16 \times 10^{21}$ V/m^2 and $\eta^D = 0$ for D. Nevertheless, in both cases, the forces on the Ta's nearest oxygen neighbors are very significant, and then we must find the equilibrium structures for the systems In_2O_3:Ta(C) and In_2O_3:Ta(D).

After full structural relaxation we found that the impurity's oxygen nearest neighbors relax inward along the Ta−ONN directions, giving Ta−ONN distances (d_{NN}) about 10% shorter than those corresponding to the pure In_2O_3 system. These contractions are due to the smaller ionic radius of Ta relative to that of the In atom that it replaces (0.65 and 0.80 Å, respectively).[57] In Table 1 we present the d_{NN} distances for the different charge states considered, calculated with LDA. We found that in Ta-doped In_2O_3 the contractions of the Ta−ONN bonds practically do not depend on the charge state of the cell. Similar results are obtained using WC-GGA. We checked that the structural distortions produced by the impurity are extremely local, and mainly affect the positions of the ONNs atoms surrounding Ta. Each Ta atom has 12 In atoms as next nearest neighbors, whose positions slightly change when we allow the full relaxation (their distances to the impurity increase in less than 0.5% of those corresponding to the pure In_2O_3 system). This result shows that the Ta atom tends to locally reconstruct the environment that it has in its own oxide TaO_2 (in which the Ta atom is 6-fold O coordinated and $d_{NN} = 2.02$ Å),[58] as it was observed for Ta in other host oxides.[27,35,40,59]

In parts b and c of Figure 2, we show the DOS for In_2O_3:Ta(D) and In_2O_3:Ta(C) systems, respectively, after full structural relaxation. Comparing these DOS with that of the pure In_2O_3 system (Figure 2a), we see that unfilled Ta-5d impurity states appear about 2 eV over the CB minimum (see

Table 1. Predicted V_{33}, Asymmetry Parameter η, and Ta−ONN Bond-Lengths d_{NN} Obtained for the Relaxed Structures and the Different Charge States of the Cell Considered[a]

	site C			site D		
	V_{33} (10^{21} V/m^2)	η	d_{NN} (Å)	V_{33} (10^{21} V/m^2)	η	d_{NN} (Å)
In_2O_3:Ta^0	−17.4	0.13	1.95, 1.95, 2.12	+19.9	0.00	2.02
In_2O_3:Ta^{1+}	−17.5	0.12	1.95, 1.96, 2.13	+20.9	0.00	2.00
In_2O_3:Ta^{2+}	−17.4	0.10	1.96, 1.96, 2.13	+20.8	0.00	2.01
exp. (this work)	16.6(4)	0.160(4)	2.12, 2.19, 2.21	19.0(4)	0	2.19

[a]Each d_{NN} value has multiplicity of two in the case of site C and six in the case of site D. The experimental results of this work are shown. The sign of V_{33} cannot be determined in standard TDPAC experiments. The cation−ONN bond-lengths for both sites in pure In_2O_3 are also quoted in the last row for comparison.

DOI: 10.1021/acs.jpcc.5b11155
J. Phys. Chem. C 2016, 120, 5640−5650

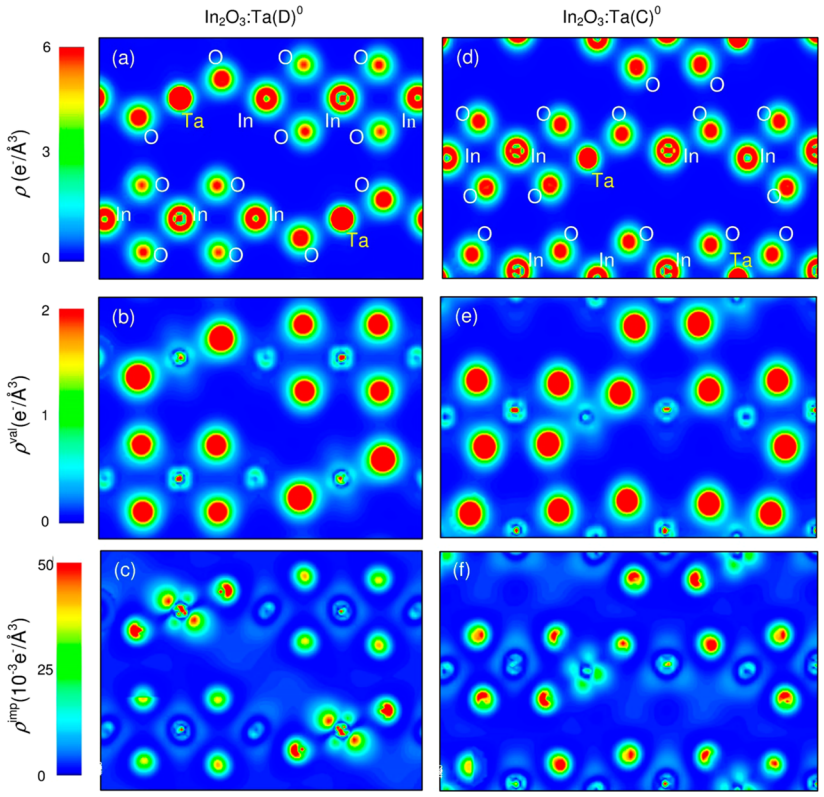

Figure 4. Total electron density $\rho(\mathbf{r})$ and partial densities $\rho^{val}(\mathbf{r})$ and $\rho^{imp}(\mathbf{r})$ for (a–c) In_2O_3:Ta(D)^0 over the (−101) plane, and (d–f) In_2O_3:Ta(C)^0 over the (101) plane. Different electron density scales were used to optimize visibility in each graph.

the peaks indicated in Figure 2, parts b and c). According to the obtained DOS for each site, the doped system is n-type metallic, with the CB bottom states partially filled. These states are just below the unfilled Ta-5d peaks, and are due to the In-5s, O-2p, and Ta-5d orbitals, as described in detail in the atom-projected partial DOS (PDOS) near the CB minimum (Figure 3, parts b and c). As can be seen, the lower region of the filled donor states are dominated by the O atoms, with a contribution of the In states, while the upper part of this region (nearer to the Fermi level, E_F) is mainly due to the Ta states.

The integration of the total DOS of Figure 2, parts b and 2c, in the occupied CB states energy region (from 7.0 eV to E_F) gives a value of 2.0 electrons, in agreement with the nominal double donor character of the substitutional Ta impurity in In_2O_3. The successive removal of electrons from the cell produces the displacement of the Fermi level toward lower energies, in such a way that when two electrons are removed from the cell the resulting system becomes insulator. From the analysis of the atom-projected PDOS we found that about 75% of the 2 electrons that fill the CB impurity states of Figure 2, parts b and c, is located at the ONN spheres. Only 4% of this charge is located at the Ta impurity atom, and the rest is distributed among the In cations and the rest of the oxygen atoms of the cell. The contribution of the interstitial region is practically negligible. These results can also be showed by analyzing the spatial distribution of the electronic charge. To this respect, in Figure 4 we plot different projections of the electron density $\rho(\mathbf{r})$ for both In_2O_3:Ta(D) and In_2O_3:Ta(C) systems. In Figure 4, parts a and d, the total $\rho(\mathbf{r})$ for both systems help to identify the position of the Ta impurity in the plane selected for each cationic impurity site. Also, the spherical distribution of the charge around In, O, and Ta atomic sites let us infer that their atomic states are strongly localized, in agreement with the ionicity of this oxide. Figures 4, parts b and e, show the projections of the electron density $\rho^{val}(\mathbf{r})$ corresponding to the valence states (from 0 to 5.7 eV, see Figure 2, parts b and c). The high relative intensity of $\rho^{val}(\mathbf{r})$ at the O atomic sites shows that the VB is mainly composed by the O-2p states, in agreement with the DOS shown in Figure 2, and reinforces the weak character of covalent bonding with the cations. Finally, Figure 4, parts c and f, show the electron density $\rho^{imp}(\mathbf{r})$ corresponding to the energy range of the occupied impurity states (from 7 eV to E_F). As can be seen, there is a significant contribution of the ONN atoms to this energy region, in agreement with the values calculated by integration of atom-resolved occupied states at the CB below E_F, showing that the 2 electrons that fill the impurity states are not mainly localized at the Ta impurity.

As mentioned above, the presence of the impurity produces structural relaxations (see Table 1 for a comparison with the unrelaxed d_{NN} bond-lengths) and, in addition, it modifies the local electronic structure of the Ta probe. The sum of both effects produces, in Ta-doped In_2O_3, EFG values that are practically independent of the charge state of the cell (see Table 1). For these relaxed structures, V_{33} at Ta(C) site is practically independent of the charge state of the cell, while the variations at Ta(D) site are below 5%, which are within the precision limit of the calculation.[34] This behavior indicates that the fraction of charge removed from the Ta sphere (around 0.08 electrons, as mentioned above) is nearly spherical and practically does not affect the EFGs at the impurity sites.

The negligible difference among the predicted EFGs as a function of the charge state of the cell (see Table 1) cannot be resolved in a TDPAC experiment. This implies that the charge

DOI: 10.1021/acs.jpcc.5b11155
J. Phys. Chem. C 2016, 120, 5640−5650

state of the ^{181}Ta impurity in real samples cannot be determined through the comparison between the *ab initio* calculated and measured EFG. In order to solve this problem, we determined the charge state of the impurity that gives the lowest energy of the doped system. In this sense, we calculated the defect formation energy (E_f) for In_2O_3:Ta^0, In_2O_3:Ta^{1+} and In_2O_3:Ta^{2+}, for Ta at both cationic sites C and D, following the formalism described in detail in refs 32 and 60. For each cationic site, we calculated E_f as a function of the charge state of the cell using

$$E_f(In_2O_3{:}\ Ta)^q = E(In_2O_3{:}\ Ta)^q - E(In_2O_3) + \mu^*_{In} + \frac{1}{2}\Delta_f H^{In_2O_3} - \mu^*_{Ta} - \frac{1}{2}\Delta_f H^{Ta_2O_5} + q(\varepsilon_F + \varepsilon'_\nu) \quad (2)$$

In this expression $\Delta_f H$ are the enthalpy formations, μ^* are the metallic crystal total energy per atom, ε_F is the Fermi energy at the band gap relative to the top of the VB energy ε'_ν, with $0 \le \varepsilon_F \le \varepsilon_g$ (ε_g is the band gap energy), and $\varepsilon'_\nu = \varepsilon_\nu + \delta_q$, with ε_ν the top of the VB energy of the pure In_2O_3 system and δ_q lines ups the band structures of the bulk material with and without impurity. The obtained results (see Figure 5) show that the In_2O_3:Ta^{2+} system is the most stable for both sites and all values of ε_F, from 0 to ε_g.

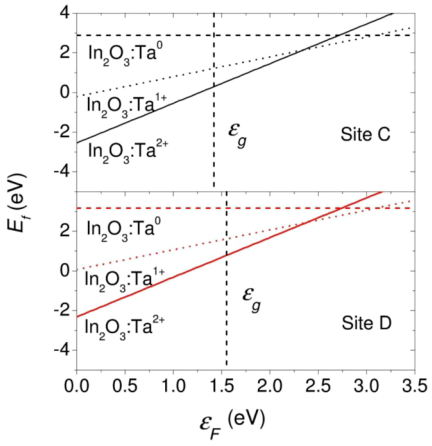

Figure 5. Defect formation energies E_f as a function of the Fermi energy level ε_F for In_2O_3:Ta(C)^q (upper) and In_2O_3:Ta(D)^q (lower), with $q = 0$ (dashed line), $q = +1$ (dotted line), and $q = +2$ (solid line). The energy band gap ε_g is indicated with a vertical dashed line.

An important result to point out is that the *ab initio* predicted asymmetry parameter η for the highly asymmetric site C is much lower than the value estimated from the analysis of the geometry of this cationic site ($\eta^C > 0.5$), and also compared to the experimental η values observed in the rest of the *bixbyite* sesquioxides with lattice parameters larger than that of In_2O_3. In addition, the predicted ratio $V_{33}{}^D/\ V_{33}{}^C$ is close to 1, while the experimental ratio for all the *bixbyites* mentioned above is close to 2.

Finally, we investigated the origin of the EFG and its dependence with the charge state of the cell considering the different orbital contributions within the atomic sphere of the Ta impurity. Using the FP-APW+lo method, we can decompose the nonspherical electron density of the valence and semicore electrons according to the different orbital symmetries.[55] We found that for all charge states of the cell the main contribution to V_{33} has p character, and it practically does not change from one charge state to another. As it is well-known this behavior can be understood by the fact that the first node of the p wave function is at shortest distance from the nucleus.[55] On the other hand, the very small changes observed in the total V_{33} value on the charge state of the cell are due to changes in the d contribution. Therefore, the resulting total V_{33} is practically independent of the charge state of the cell, as already observed for other Ta-doped binary oxides.[27,35] This behavior is due to an homogeneous remotion of d-type electronic charge.

In order to get a deeper insight on this subject, we inspected closer the relative weights of the p and d contributions to V_{33} and their charge state dependence using first the pure In_2O_3 atomic positions fixed (unrelaxed structure). Opposite to the behavior observed in the relaxed systems, V_{33} strongly depends on the charge state of the cell. This behavior is due to an important change in the Ta-d contribution to V_{33}, while the dominant p contribution is almost constant for different charge states. Using the unrelaxed structure, we found that the Ta-5d peaks that are localized at higher energies with respect to E_F in the relaxed In_2O_3:Ta system (see Figures 2 and 3) are in this case below E_F and, therefore, partially filled. The removal of 1 or 2 electrons lead to an strong change in the occupation of the d_{z^2} orbital, affecting the total $V_{33}{}^C$ and $V_{33}{}^D$ values and the η^C parameter.[27,35] This effect is not present when the structure is relaxed, as we already showed, thus resulting in the constancy of the EFG upon changes of the charge state of the impurity.

IV. EXPERIMENTAL RESULTS

A. Previous TDPAC Experiments in ^{181}Ta-Doped In_2O_3.

We will review here the experimental TDPAC results reported in the literature for ^{181}Ta-doped In_2O_3. Previous experiments using (^{181}Hf →)^{181}Ta as probe were performed by Vercesi et al.[41] and Rentería et al.[42]

Vercesi et al. found for ^{181}Hf(→^{181}Ta)-implanted In_2O_3 film samples two hyperfine interactions (see HFI I and HFI II in Table 2). These interactions were associated with probes located at substitutional cation sites C and D, respectively. This assignment of the hyperfine interactions was based in simple models, taking into account the *bixbyite* crystal structure and a homogeneous population of both cationic sites, obtaining a relative population $f^C/f^D \approx 3$, as observed in ^{111}Cd-doped In_2O_3.[13−17] Nevertheless, contrarily to that observed in the EFG systematics found for the ^{111}Cd probe,[34,48] they found that both quadrupole interactions present similar V_{33} values ($V_{33}{}^C \approx V_{33}{}^D$). Moreover, the interaction associated with the axially symmetric site D present an asymmetry parameter $\eta^D = 0.35$, while for the asymmetric site C $\eta^C = 0.1$. The authors attributed these disagreements with the expected values to strong structural local distortions of the Ta environment but still located in both cationic sites of the *bixbyite* structure.[41]

Later, Rentería et al. studied samples prepared by different methods and with different initial degrees of crystallinity. In all the experiments, four hyperfine interactions were necessary to account for the TDPAC spectra (see Table 2). Based in the geometry of both cation sites in the *bixbyite* structure and in the previous studies using ^{111}Cd as probe, one of these interactions characterized by $\eta = 0.15$ (see HFI 1 in Table 2) was associated with probes located at the axially symmetric site D. The interaction characterized by $\eta > 0.5$ (see HFI 2 in Table 2) was associated with probes located at the asymmetric site C. With this assignment the relative population $f^C/f^D \ll 1$. In other words, the probes do not occupy the cationic sites in a

DOI: 10.1021/acs.jpcc.5b11155
J. Phys. Chem. C 2016, 120, 5640−5650

Table 2. Results of the Hyperfine Parameters Coming from Previous TDPAC Experiments

sample	site assign.	f (%)	ω_Q (Mrad/s)	η	δ (%)	V_{33} (10^{21} V/m^2)
crystalline film implanted[a]	HFI I	74(1)	146.6(2)	0.11(1)	0.00(1)	16.35(2)
	HFI II	26(4)	145.6(7)	0.35(1)	0.01(1)	16.24(8)
chemically prepared neutron irradiated[b]	HFI 1	45(2)	146.2(2)	0.149(7)	0.8(1)	16.31(2)
	HFI 2	35(8)	110.7(8)	0.6(9)	9(1)	12.35(9)
	HFI 3	12(2)	163.9(6)	0.05(7)	1.9(7)	18.28(7)
	HFI 4	8(1)	161(2)	0.84(2)	3(1)	17.9(2)
crystalline film implanted[b]	HFI 1	61(2)	147.0(1)	0.150(6)	0.4(1)	16.40(1)
	HFI 2	9(2)	115.3(7)	0.54(2)	0.9(9)	12.86(8)
	HFI 3	25(3)	164.3(5)	0.14(2)	2.0(5)	18.33(6)
	HFI 4	5(1)	157(1)	0.84(2)	0.1(8)	17.5(1)
amorphous film implanted[b]	HFI 1	61(4)	146.5(2)	0.157(7)	1.1(2)	16.34(2)
	HFI 2	8(3)	107.5(6)	0.75(2)	0(1)	11.99(7)
	HFI 3	19(6)	164(1)	0.18(3)	3(1)	18.3(1)
	HFI 4	12(2)	158(2)	0.66(3)	3(1)	17.6(2)

[a]Reference 41 [b]Reference 42

homogeneus way, being site D the preferential site. This *inversion* in the site population is not observed in the systematics found for the ^{111}Cd probe.[34,48] Finally, the other two interactions (HFI 3 and HFI 4) were associated with probes located at defect cationic sites. Hence, both experiments presented apparently divergent hyperfine characterizations for ^{181}Ta probes localized at both cationic sites of the structure.

B. Present TDPAC Experiments. Because of the strong controversy between the EFG predicted by the FP-APW+lo calculations and the previous divergent experimental results in ^{181}Ta-doped In_2O_3,[41,42] we performed new careful TDPAC experiments with high statistics in ^{181}Hf-implanted In_2O_3 polycrystalline samples with high crystallinity.

The TDPAC experiments were carried out using a spectrometer containing four coplanar BaF_2 scintillator detectors in a 90° geometry arrangement with a fast−fast coincidence logic. This spectrometer presents particularly high efficiency and time resolution for the 133−482 keV $\gamma-\gamma$ cascade of the ^{181}Ta probe.[61]

The initial sample was prepared following a standard chemical procedure. High purity metallic indium was dissolved by reacting with nitric acid (HNO_3) in an aqueous distilled solution. This reaction was accelerated heating the solution at 373 K in order to obtain aqueous indium nitrate ($In(NO_3)_3 \cdot 6H_2O$). During heating at 373 K, water is first evaporated and then the nitrous acid (HNO_3). After this, the resulting white powder was calcined at 773 K in order to obtain the final pale yellow powder (In_2O_3). Finally, in order to remove defects and enhance its crystallinity, the resulting powder was thermally treated at 1273 K in air for 1 h. The high crystallinity of the sample was confirmed by X-ray diffraction (XRD) experiments. All the In_2O_3 characteristic lines were found in the XRD pattern, as shown in Figure 6. In_2O_3 policrystalline pellets were obtained pressing 100 mg of the obtained powder and sintering them for 1 h at 1273 K. In order to dope the sample with ^{181}Ta probes, one pellet was exposed to a flux of ^{181}Hf ions in the accelerator facility of the Helmholtz-Institut für Strahlen- und Kernphysik (H-ISKP, Bonn, Germany). The implantation energies were of the order of 160 keV, and the total calculated dose was 3.1×10^{12} ions/cm^2. After implantation, the pellet underwent isochronal thermal treatments in air for 1h at T_a= 673, 1073, and 1273 K. After this, it was manually grinded in an agate mortar and heated in air during 30 min at 1273 K and 1 h at 1373 K.

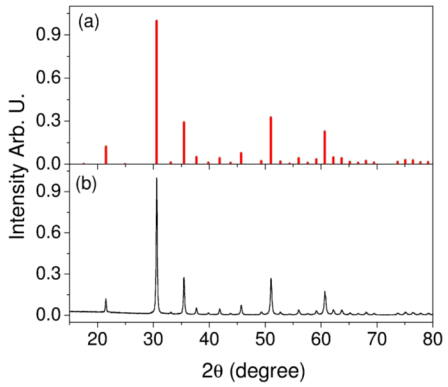

Figure 6. Comparison between (a) reported XRD lines[47] and (b) the experimental diffraction pattern.

The TDPAC measurements were performed at room-temperature in air after implantation and after each step of the series of thermal treatments mentioned above. Finally, a TDPAC measurement in air at high temperature (T_m = 1273 K) was performed. Figure 7 shows selected experimental $R(t)$ spectra (left) and their corresponding Fourier transforms (right), for ^{181}Hf-implanted In_2O_3 pellet as implanted (Figure 7a), after the 673 K thermal treatment (Figure 7b), after the treatment at 1273 K after grinding (Figure 7c), and the final measurement performed at 1273 K in air (Figure 7d).

In the as implanted spectrum, there is a major hyperfine interaction (f = 91(6)%) with parameters $V_{33} = 13(2) \times 10^{21}$ V/m^2 and η = 0.6(2), and a high frequency distribution (δ = 95%), responsible for the strong damping of the spectrum. After each annealing step two well-defined (δ< 3%) hyperfine interactions account for the whole spectra. Parts b and c of Figure 7 reflect the signal improvement upon the annealing treatments. V_{33} and η for both interactions practically do not change during the annealing series and their V_{33} distributions δ slightly decreases with successive annealings (the largest V_{33} distribution decrease is produced after the 1073 K treatment). These hyperfine parameters do not change upon grinding, independently of the annealing temperature performed before each measurement. These two new interactions were associated with probes located at defect-free cationic sites C and D of the crystalline *bixbyite* structure. The corresponding hyperfine parameters for all relevant spectra are listed in Table 3. It is

DOI: 10.1021/acs.jpcc.5b11155
J. Phys. Chem. C 2016, 120, 5640−5650

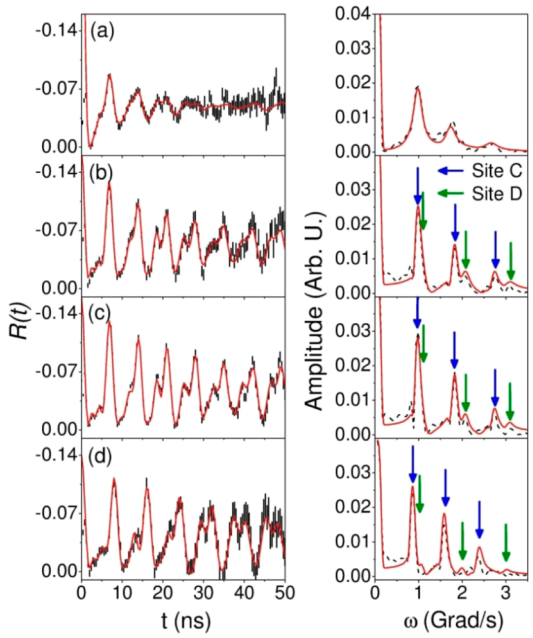

Figure 7. TDPAC spectra (left) and their corresponding Fourier transformed spectra (right) measured in air at room temperature on (a) the as implanted In_2O_3:($^{181}Hf \rightarrow$)^{181}Ta sample, (b) after the 673 K thermal treatment step, and (c) after the 1273 K thermal treatment step after grinding, and (d) measured at T_m = 1273 K (see text). The red solid lines are least-squares fits of eq 1 to the $R(t)$ spectra (left), and their corresponding Fourier transform (right). The ω_n frequencies associated with probes located at the defect-free cationic sites C and D of the structure are the triplets indicated by arrows in the Fourier spectra.

well-known that the thermal annealing treatments following ion implantation remove the radiation damage and favor the replacement of host cations by TDPAC probes.[27,48,62] Considering this, the initial interaction assignment was done based on the relative abundance of both inequivalent cations sites of the *bixbyite* structure and the intensities of the obtained hyperfine interactions. So, the dominant hyperfine interaction was assigned to probes localized at cationic site C, and the minority interaction to probes localized at site D. With these assignments, the axially symmetric interaction is in agreement with the axial symmetry of site D. Even though V_{33}^D is not twice as large as V_{33}^C as in the rest of ^{181}Ta-doped and ^{111}Cd-doped *bixbyites*,[12] V_{33}^D is still larger than V_{33}^C. According to the values presented in Table 3, the ratio f^C/f^D is 2.6, 4.9, and 5.2 after the thermal annealings performed at 673, 1073, and 1273 K, respectively. The two last ratios are larger than the crystallographic relative abundance of sites C and D in the *bixbyite* structure (3:1). The deviations from the value f^C/f^D = 3, which would correspond to a homogeneous population of the cationic sites by the TDPAC probe, are consistent with the variations previously observed in other isomorphous oxides.[12,62] The present experimental value points to a preference of the ^{181}Hf atoms for the asymmetric site C, in perfect agreement with the site preference predicted by the FP-APW+lo total energy calculations of Hf atoms localized at each cationic site of In_2O_3, presented in section III.B. It should be noted here that the V_{33} values decrease when the sample is measured at high temperature, in particular that corresponding to the asymmetric site C (7%), effect that could be attributed to the lattice expansion. In addition, the largest ratio f^C/f^D= 9 obtained at T_m= 1273 K points to a migration of ^{181}Hf atoms from sites D to sites C, promoted by the continuous thermal energy supplied during the TDPAC measurement.

Beyond the fact that the ratio between the V_{33} values that characterize both hyperfine interactions, i.e. 1.14, is not exactly that expected from the rest of the EFG systematics in ^{181}Ta-doped *bixbyites* (see Figure 8), there is another unexpected result. In effect, the measured asymmetry parameter for site C is extremely low (η^C = 0.160(4)), compared to that predicted by point-charge model calculations and the experimental values observed for the rest of the EFG systematics. Nevertheless, the FP-APW+lo calculations could predict these behaviors: as shown in Table 1, all the predicted hyperfine parameters are in

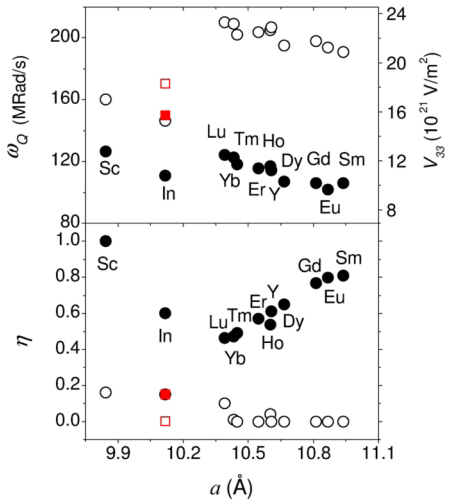

Figure 8. Experimental ω_Q and η values as a function of the lattice parameter a in *bixbyites* measured at ^{181}Ta atoms localized at cation sites D (white circles) and C (black circles).[48] Open (site D) and filled (site C) red squares correspond to the present experimental In_2O_3 characterization.

Table 3. Results of Least-Squares Fits of Equation 1 to the $R(t)$ Spectra Taken at Room Temperature in Air after Each Annealing Treatment in Air at T_a[a]

	site C					site D				
T_a (K)	f (%)	ω_Q (Mrad/s)	η	δ (%)	V_{33} (10^{21} V/m^2)	f (%)	ω_Q (Mrad/s)	η	δ (%)	V_{33} (10^{21} V/m^2)
673	72(5)	149.3(4)	0.166(7)	1.8(3)	16.7(4)	28(2)	170.2(9)	0.05(7)	2.6(9)	19.0(4)
1073	83(3)	149.1(2)	0.159(6)	1.6(2)	16.6(4)	17.3(7)	170.7(6)	0	0.8(6)	19.0(4)
1273	84(2)	149.0(2)	0.160(4)	1.4(1)	16.6(4)	15.7(4)	170.0(5)	0	0.7(5)	19.0(4)
1373	90(1)	129.4(2)	0.202(5)	1.4	14.4(4)	10.1(2)	166(1)	0.00(3)	1.04	18.6(8)

[a]The T_a = 1273 K spectrum was measured after grinding. Last row corresponds to the high-temperature measurement at T_m = 1273 K. When no errors are quoted it means that the parameter was kept fixed during the fitting procedure.

DOI: 10.1021/acs.jpcc.5b11155
J. Phys. Chem. C 2016, 120, 5640−5650

excellent agreement with our experimental results measured at room temperature.

In summary, the two obtained hyperfine interactions can be now undoubtedly assigned to ^{181}Ta probes located at defect-free cationic sites C and D of the *bixbyite* structure.

V. COMPARISON WITH PREVIOUS EXPERIMENTS

The combination between accurate TDPAC experiments performed in a ^{181}Hf-implanted In_2O_3 policrystalline sample with a high degree of crystallinity and the DFT electronic structure calculations allowed a final hyperfine characterization of ^{181}Ta impurities localized at both cationic sites C and D of the free of defects *bixbyite* structure. Even though the hyperfine interactions assignment was not trivial and divergent with respect to those proposed in previous experiments, there are some results in common among the different experiments but they differ in their interpretation. A remarkable result in our experiment is the low value of η^C, distant from the expected value considering this site symmetry. This result can be linked to that obtained by Vercesi et al. in a ^{181}Hf($\rightarrow^{181}$Ta)-implanted In_2O_3 film sample, where $\eta^I = 0.11(1)$,[41] assigned to site C in that paper. However, in that experiment it was obtained $V_{33}{}^I \approx V_{33}{}^{II}$, and $\eta^{II} = 0.35(1)$, results that were explained by a strong distortion of both surroundings for the impurity, in such a way that the local environment could be similar for the probe located at both cationic sites of the structure (see Table 2). Under the light of the present results coming from the *ab initio* calculations and the new experiment we can conclude that HFI I in that paper can be assigned to probes located at site C free-of-defects. On the other hand, HFI II, whose parameters differ strongly with our results, points to a defect trapped at the symmetric site in that sample. Afterward, the results obtained by Vercesi et al.[41] could not be reproduced during the experiments performed by Rentería et al.,[42] where four interactions were necessary to fit the TDPAC spectra. Rentería et al. proceeded with an interaction assignment considering the two more intense interactions (in the chemically prepared sample), which contributed with more than 70% to the $R(t)$ spectra. They assumed that these two interactions should correspond to ^{181}Ta probes located at sites C and D, and performed an assignment that fulfilled the conditions $V_{33}{}^{II} < V_{33}{}^{I}$ and $\eta^{II} \gg \eta^I \approx 0.15$ (see Table 2). However, by doing so, their assignment gave a ratio $f^C/f^D < 1$, i.e., an anomalous *inversion* of the cationic site population. Among the four interactions, the third more intense has parameters $\eta^3 \approx 0.1$ and $V_{33} \approx 18.3 \times 10^{21}$ V/m^2 (see Table 2), which was associated with a probe environment where an ^{181}Hf atom is present in the second coordination sphere of the ^{181}Ta atom. If we forget the assignment performed by Rentería et al. and we assign HFI 3 to probes located at site D, and HFI 1 to probes located at site C (see Table 2), the experimental results are consistent with those presented in the present work. In fact, η^3 is null only in the chemically prepared sample and slightly higher in the implanted ones. Nevertheless, the non negligible additional hyperfine interactions observed in that experiments point to the existence of an additional defect structure in the investigated samples. It should be mentioned that with the proposed hyperfine interaction assignment the anomalous *inversion* of the cation site population is removed.

The double experimental-theoretical approach applied in the present work enabled not only the final EFG characterization in ^{181}Ta-doped In_2O_3 but also to solve the controversies among all the reported experiments.

VI. CONCLUSIONS

In this work, we have presented a detailed FP-APW+lo study of the structural, electronic, and hyperfine properties in the (^{181}Hf $\rightarrow$)^{181}Ta-doped In_2O_3 semiconductor, and new TDPAC experiments were analyzed in order to establish a definitive hyperfine characterization at ^{181}Ta impurities localized at substitutional defect-free cation sites of the *bixbyite* structure.

The FP-APW+lo calculations showed that when the Ta atom substitutes an In atom, the resulting system is metallic due to the population of the CB bottom states. The presence of the impurity induces the appearance of Ta-5d states as partially filled donor levels. In order to simulate the different possible ionization states of the impurity, we analyzed three charge states of the unit cell by removing electrons from it. We found that only a very small fraction of the removed electrons is localized at the atomic sphere of the impurity, being the major part of this charge distributed among its ONN. The substitutional Ta atom tries to reconstruct the environment that it has in its own oxide, producing anisotropic contractions of the cation-ONN bond-lengths. These structural distortions are of paramount importance in order to get a complete description of the impurity-host system, in particular for an accurate prediction of the EFGs.

Experimentally, two monochromatic hyperfine interactions were found in the dedicated TDPAC experiments performed onto ^{181}Hf-implanted In_2O_3 policrystalline samples, associated with ^{181}Ta impurities localized at both inequivalent cationic site of the structure. The combination of accurate experiments in samples with high crystallinity with first-principles calculations was necessary in order to obtain a final characterization of the EFG in ^{181}Ta-doped In_2O_3, to understand the origin of the EFG and to solve controversies raised among all the previously reported experiments.

In this respect, the EFG predictions corresponding to the relaxed structures (independently of the simulated charge state of the cell) are in excellent agreement with the values coming from our TDPAC experiments. The constancy of the EFG upon changes in the charge state of the impurity resides on the fact that the sharp 5d donor levels introduced by the Ta impurity are localized above the Fermi level when the structure is relaxed. In order to predict the correct charge state of the impurity we performed defect formation energy calculations, obtaining that the insulating In_2O_3:Ta^{2+} system gives the lowest formation energy, for the impurity located at both cationic sites. The calculations gave support to the new EFG measurements and their interpretation, confirming the unexpected extremely low asymmetry parameter value for the asymmetric site C ($\eta^C \approx 0.16$). Also, the *inversion* of the cationic sites population proposed for ^{181}Hf($\rightarrow^{181}$Ta) in *bixbyites* as the lattice parameter becomes shorter has to be abandoned (at least for *bixbyites* with lattice parameters larger than that of In_2O_3). Additionally, the *ab initio* calculations predict that V_{33} has predominantly p character at both crystallographic sites, and provide a way to infer its sign at each cationic site, which cannot be determined in standard TDPAC experiments.

In summary, we obtained a definitive result for the EFGs at ^{181}Ta impurities localized at both C and D defect-free cationic sites of the In_2O_3 semiconductor. The obtained hyperfine parameters suggest that the TDPAC probe modifies the local structure, in particular that of site C. Theoretically, the FP-APW+lo calculations confirmed this result: when a Ta atom substitutes an In atom, the cationic environment where the

DOI: 10.1021/acs.jpcc.5b11155
J. Phys. Chem. C 2016, 120, 5640−5650

impurity is placed changes drastically, and these structural distortions need to be considered in order to correctly predict the EFGs. These results show that, for this system, the combination of experiments with first-principles calculations is essential to allow a complete understanding of the EFGs at the Ta impurity sites.

■ ASSOCIATED CONTENT

Supporting Information

The Supporting Information is available free of charge on the ACS Publications website at DOI: 10.1021/acs.jpcc.5b11155.

Complete author list of refs 2, 19, and 20 (PDF)

■ AUTHOR INFORMATION

Corresponding Author

*(D.R.) E-mail: richard@fisica.unlp.edu.ar.

Notes

The authors declare no competing financial interest.

■ ACKNOWLEDGMENTS

This work was partially supported by Consejo Nacional de Investigaciones Científicas y Técnicas (CONICET) under Grant No. PIP0002, Argentina, and the Third World Academy of Sciences (TWAS), Italy (RGA 97-057). The ^{181}Hf implantations carried out at the H-ISKP of Bonn University (Germany) are kindly acknowledged. This research made use of the HP-Parallel-Computing Bose Cluster, and the computational facilities of the Physics of Impurities in Condensed Matter (PhI) group at IFLP and Departamento de Física (UNLP). G.N.D., L.A.E, and M.R. are members of CONICET, Argentina.

■ REFERENCES

(1) Wang, Ch. Y.; Cimalla, V.; Romanus, H.; Kups, Th.; Niebelschütz, M.; Ambacher, O. Tuning of Electrical and Structural Properties of Indium Oxide Films Grown by Metal Organic Chemical Vapor Deposition. *Thin Solid Films* **2007**, *515*, 6611−6614.

(2) Chen, P.-C.; Shen, G.; Chen, H.; Ha, Y.; Wu, C.; Sukcharoenchoke, S.; Fu, Y.; Liu, J.; Facchetti, A.; Marks, T. J.; et al. High-Performance Single-Crystalline Arsenic-Doped Indium Oxide Nanowires for Transparent Thin-Film Transistors and Active Matrix Organic Light-Emitting Diode Displays. *ACS Nano* **2009**, *3*, 3383−3390.

(3) Mori, S.; Asano, A. Light Intensity Independent Electron Transport and Slow Charge Recombination in Dye-Sensitized In_2O_3 Solar Cells: In Contrast to the Case of TiO_2. *J. Phys. Chem. C* **2010**, *114*, 13113−13117.

(4) Sobajima, Y.; Muto, H.; Shinohara, Y.; Sada, C.; Matsuda, A.; Okamoto, H. Fundamental Properties of Titanium-doped Indium Oxide and Its Application to Thin-Film Silicon Solar Cells. *Jpn. J. Appl. Phys.* **2012**, *51*, 10NB05.

(5) Golovanov, V.; Mäki-Jaskari, M. A.; Rantala, T. T.; Korotcenkov, G.; Brinzari, V.; Cornet, A.; Morante, J. Experimental and Theoretical Studies of Indium Oxide Gas Sensors Fabricated by Spray Pyrolysis. *Sens. Actuators, B* **2005**, *106*, 563−571.

(6) Korotcenkov, G.; Stetter, J. R. Comparative Study of SnO_2- and In_2O_3-Based Ozone Sensors. *ECS Trans.* **2007**, *6*, 29−41.

(7) Philip, J.; Punnoose, A.; Kim, B. I.; Reddy, K. M.; Layne, S.; Holmes, J. O.; Satpati, B.; LeClair, P. R.; Santos, T. S.; Moodera, J. S. Carrier-Controlled Ferromagnetism in Transparent Oxide Semiconductors. *Nat. Mater.* **2006**, *5*, 298−304.

(8) Peleckis, G.; Wang, X.; Dou, S. X. High Temperature Ferromagnetism in Ni-doped In_2O_3 and Indium-Tin Oxide. *Appl. Phys. Lett.* **2006**, *89*, 022501.

(9) Peleckis, G.; Wang, X. L.; Dou, S. X. Room-Temperature Ferromagnetism in Mn and Fe Codoped In_2O_3. *Appl. Phys. Lett.* **2006**, *88*, 132507.

(10) Qi, S.; Jiang, F.; Fan, J.; Wu, H.; Zhang, S. B.; Gehring, G. A.; Zhang, Z.; Xu, X. Carrier-Mediated Nonlocal Ferromagnetic Coupling Between Local Magnetic Polarons in Fe-doped In_2O_3 and Co-doped ZnO. *Phys. Rev. B: Condens. Matter Mater. Phys.* **2011**, *84*, 205204.

(11) Semin, G. K. On Solving Secular Equations for Half-Integer Spins (I = 5/2, 7/2, and 9/2) in NQR Spectroscopy. *Russ. J. Phys. Chem. A* **2007**, *81*, 38−46 and references therein.

(12) Pasquevich, A. F.; Rentería, M. Impurity Centers in Oxides Investigated by γ-γ Perturbed Angular Correlation Spectroscopy and Ab Initio Calculations. *Defect Diffus. Forum* **2011**, *311*, 62−104.

(13) Desimoni, J.; Bibiloni, A. G.; Mendoza-Zélis, L.; Pasquevich, A. F.; Sánchez, F. H.; López-García, A. Kinetics Studies and Oxide Characterization in the Internal Oxidation of AgIn Alloys. *Phys. Rev. B: Condens. Matter Mater. Phys.* **1983**, *28*, 5739−5745.

(14) Bibiloni, A. G.; Desimoni, J.; Massolo, C. P.; Mendoza-Zélis, L.; Pasquevich, A. F.; Sánchez, F. H.; López-García, A. Temperature Dependence of Electron-Capture Aftereffects in the Semiconductor In2O3. *Phys. Rev. B: Condens. Matter Mater. Phys.* **1984**, *29*, 1109−1111.

(15) Bolse, W.; Uhrmacher, M.; Kesten, J. The EFG of the In-O-Bond In_2O_3, AgO and Ag_2O. *Hyperfine Interact.* **1987**, *35*, 931−934.

(16) Habenicht, S.; Lupascu, D.; Uhrmacher, M.; Ziegeler, L.; Lieb, K. P. PAC-Studies of Sn-doped In_2O_3: Electronic Defect Relaxation Following the ^{111}In(EC) ^{111}Cd-Decay. *Z. Phys. B: Condens. Matter* **1996**, *101*, 187−196.

(17) Muñoz, E. L. Estudio Experimental y de Primeros Principios de Interacciones Hiperfinas Dinámicas en Óxidos Semiconductores Dopados con Impurezas (^{111}In(EC)→)^{111}Cd. Ph.D. Thesis, Universidad Nacional de La Plata: La Plata, Argentina, March 2011. http://sedici.unlp.edu.ar/handle/10915/2628 (accessed February 5, 2016).

(18) Karazhanov, S. Zh.; Ravindran, P.; Vajeeston, P.; Ulyashin, A.; Finstad, T. J.; Fjellvåg, H. Phase Stability, Electronic Structure, and Optical Properties of Indium Oxide Polytypes. *Phys. Rev. B: Condens. Matter Mater. Phys.* **2007**, *76*, 075129.

(19) Walsh, A.; Da Silva, J. L. F.; Wei, S. − H.; Körber, C.; Klein, A.; Piper, L. F. J.; DeMasi, A.; Smith, K. E.; Panaccione, G.; Torelli, P.; et al. Nature of the Band Gap of In_2O_3 Revealed by First-Principles Calculations and X-Ray Spectroscopy. *Phys. Rev. Lett.* **2008**, *100*, 167402.

(20) King, P. D. C.; Veal, T. D.; Fuchs, F.; Wang, C. Y.; Payne, D. J.; Bourlange, A.; Zhang, H.; Bell, G. R.; Cimalla, V.; Ambacher, O.; et al. Band Gap, Electronic Structure, and Surface Electron Accumulation of Cubic and Rhombohedral In_2O_3. *Phys. Rev. B: Condens. Matter Mater. Phys.* **2009**, *79*, 205211.

(21) Medvedeva. J. E. *Combining Optical Transparency with Electrical Conductivity: Challenges and Prospects*; Wiley: Chichester, England, 2010; pp 1−29.

(22) Palandage, K.; Fernando, G. W. Role of Point Defects on Conductivity, Magnetism and Optical Properties in In_2O_3. *Phys. Lett. A* **2010**, *374*, 2879−2885.

(23) Aliabad, H. A. R.; Arabshahi, H.; Aliabadi, A. H. The Effect of Hubbard Potential on Effective Mass of Carriers in Doped Indium Oxide. *Int. J. Phys. Sci.* **2012**, *7*, 696−708.

(24) Dixit, H.; Saniz, R.; Cottenier, S.; Lamoen, D.; Partoens, B. Electronic Structure of Transparent Oxides with the Tran-Blaha Modified Becke-Johnson Potential. *J. Phys.: Condens. Matter* **2012**, *24*, 205503.

(25) Errico, L. A.; Fabricius, G.; Rentería, M.; de la Presa, P.; Forker, M. Anisotropic Relaxations Introduced by Cd Impurities in Rutile TiO_2: First-Principles Calculations and Experimental Support. *Phys. Rev. Lett.* **2002**, *89*, 055503.

(26) Errico, L. A.; Fabricius, G.; Rentería, M. Metal impurities in an oxide: Ab Initio Study of Electronic and Structural Properties of Cd in Rutile TiO_2. *Phys. Rev. B: Condens. Matter Mater. Phys.* **2003**, *67*, 144104 and references therein.

DOI: 10.1021/acs.jpcc.5b11155
J. Phys. Chem. C 2016, 120, 5640−5650

(27) Darriba, G. N.; Errico, L. A.; Eversheim, P. D.; Fabricius, G.; Rentería, M. First-Principles and Time-Differential γ-γ Perturbed-Angular-Correlation Spectroscopy Study of Structural and Electronic Properties of Ta-doped TiO_2 Semiconductor. *Phys. Rev. B: Condens. Matter Mater. Phys.* **2009**, *79*, 115213.
(28) Darriba, G. N.; Errico, L. A.; Muñoz, E. L.; Richard, D.; Eversheim, P. D.; Rentería, M. Electric-Field Gradients at Ta Donor Impurities in Cr_2O_3(Ta) Semiconductor. *Phys. B* **2009**, *404*, 2739−2741.
(29) Richard, D.; Muñoz, E. L.; Butz, T.; Errico, L. A.; Rentería, M. Electronic and Structural Properties, and Hyperfine Interactions at Sc Sites in the Semiconductor Sc_2O_3: TDPAC and Ab Initio Study. *Phys. Rev. B: Condens. Matter Mater. Phys.* **2010**, *82*, 035206.
(30) Darriba, G. N.; Muñoz, E. L.; Eversheim, P. D.; Rentería, M. Experimental and Ab Initio Study of the Nuclear Quadrupole Interaction of ^{181}Ta-probes in an α-Fe_2O_3 Single Crystal. *Hyperfine Interact.* **2010**, *197*, 207−212.
(31) Richard, D.; Muñoz, E. L.; Butz, T.; Errico, L. A.; Rentería, M. Comment on "^{45}Sc Spectroscopy of Solids: Interpretation of Quadrupole Interaction Parameters and Chemical Shifts. *J. Phys. Chem. C* **2011**, *115*, 17621−17622.
(32) Darriba, G. N.; Rentería, M.; Petrilli, H. M.; Assali, L. V. C. Site Localization of Cd Impurities in Sapphire. *Phys. Rev. B: Condens. Matter Mater. Phys.* **2012**, *86*, 075203.
(33) Muñoz, E. L.; Mercurio, M. E.; Cordeiro, M. R.; Pereira, L. F. D.; Carbonari, A. W.; Rentería, M. Dynamic Hyperfine Interactions in ^{111}In(^{111}Cd)-doped ZnO Semiconductor: PAC Results Supported by Ab Initio Calculations. *Phys. B* **2012**, *407*, 3121−3124.
(34) Richard, D.; Muñoz, E. L.; Rentería, M.; Errico, L. A.; Svane, A.; Christensen, N. E. Ab Initio LSDA and LSDA+U Study of Pure and Cd-doped Cubic Lanthanide Sesquioxides. *Phys. Rev. B: Condens. Matter Mater. Phys.* **2013**, *88*, 165206.
(35) Darriba, G. N.; Muñoz, E. L.; Errico, L. A.; Rentería, M. Ab Initio Study of Structural, Electronic and Hyperfine Properties of n-type SnO_2:Ta Semiconductor. *J. Phys. Chem. C* **2014**, *118*, 19929−19939.
(36) Richard, D.; Errico, L. A.; Rentería, M. Electronic, Structural, and Hyperfine Properties of Pure and Cd-doped Hexagonal La_2O_3 Semiconductor. *Comput. Mater. Sci.* **2015**, *102*, 119−125.
(37) Errico, L. A.; Rentería, M.; Fabricius, G.; Darriba, G. N. FLAPW Study of the EFG Tensor at Cd Impurities in In_2O_3. *Hyperfine Interact.* **2004**, *158*, 63−69.
(38) Errico, L. A.; Rentería, M.; Bibiloni, A. G.; Darriba, G. N. Temperatura Dependence of the EFG at Cd-doped Lu_2O_3: How Ab Initio Calculations can Complement PAC Experiments. *Phys. Status Solidi C* **2005**, *2*, 3576−3580.
(39) Muñoz, E. L.; Richard, D.; Errico, L. A.; Rentería, M. Ab Initio Study of the EFG Tensor at Cd Impurities in Sc_2O_3 Semiconductor. *Phys. B* **2009**, *404*, 2757−2759.
(40) Richard, D.; Muñoz, E. L.; Errico, L. A.; Rentería, M. Electric-Field Gradients at Ta Impurities in Sc_2O_3 Semiconductor. *Phys. B* **2012**, *407*, 3134−3136.
(41) Vercesi, J. A.; Bibiloni, A. G.; Massolo, C. P.; Moreno, M. S.; Pasquevich, A. F.; Freitag, K. Hyperfine Characterization of ^{181}Ta in In_2O_3. *Phys. Rev. B: Condens. Matter Mater. Phys.* **1993**, *47*, 490−492.
(42) Rentería, M.; Requejo, F. G.; Bibiloni, A. G.; Pasquevich, A. F.; Shitu, J.; Freitag, K. Perturbed-Angular-Correlation Study of the Electric-Field Gradient in ^{181}Hf-doped and Implanted Indium Sesquioxide. *Phys. Rev. B: Condens. Matter Mater. Phys.* **1997**, *55*, 14200−14207.
(43) Schatz, G.; Weidinger, A. *Nuclear Condensed Matter Physics: Nuclear Methods and Applications*; Wiley: Chichester, England, 1996.
(44) Stone, N. J. Table of Nuclear Magnetic Dipole and Electric Quadrupole Moments. *At. Data Nucl. Data Tables* **2005**, *90*, 75−176.
(45) Mendoza-Zélis, L. A.; Bibiloni, A. G.; Caracoche, M. C.; López-García, A. R.; Martínez, J. A.; Mercader, R. C.; Pasquevich, A. F. Temperature Dependence of the Electric Field Gradient at Ta Nuclei in Hafnium Pyrovanadate. *Hyperfine Interact.* **1977**, *3*, 315−320.
(46) Wyckoff, R. W. G. *Crystal Structures*; Wiley: New York, 1964; Chapter 5, Vol. 2.
(47) Marezio, M. Refinement of the Crystal Structure of In_2O_3 at Two Wavelengths. *Acta Crystallogr.* **1966**, *20*, 723−728.
(48) Errico, L. A.; Rentería, M.; Bibiloni, A. G.; Freitag, K. Electric-Field Gradients at ^{181}Ta Impurity Sites in Ho_2O_3 and Eu_2O_3 Bixbyites. *Phys. B* **2007**, *389*, 124−129 and referentes therein.
(49) Wiarda, D.; Uhrmacher, M.; Bartos, A.; Lieb, K. P. Electric Field Gradients at ^{111}Cd in Binary Oxides. *J. Phys.: Condens. Matter* **1993**, *5*, 4111−4124.
(50) Blaha, P.; Schwarz, K.; Madsen, G.; Kvasnicka, D.; Luitz, J. *WIEN2k, An Augmented Plane Wave + Local Orbitals Program for Calculating Crystal Properties*; Technical Universität: Wien, Austria, 2012.
(51) Madsen, G. K. H.; Blaha, P.; Schwarz, K.; Sjöstedt, E.; Nordström, L. Efficient Linearization of the Augmented Plane-Wave Method. *Phys. Rev. B: Condens. Matter Mater. Phys.* **2001**, *64*, 195134.
(52) Blöchl, P. E.; Jepsen, O.; Andersen, O. K. Improved Tetrahedron Method for Brillouin-Zone Integrations. *Phys. Rev. B: Condens. Matter Mater. Phys.* **1994**, *49*, 16223−16233.
(53) Perdew, J. P.; Wang, Y. Accurate and Simple Analytic Representation of the Electron-Gas Correlation Energy. *Phys. Rev. B: Condens. Matter Mater. Phys.* **1992**, *45*, 13244−13249.
(54) Wu, Z.; Cohen, R. E. More Accurate Generalized Gradient Approximation for Solids. *Phys. Rev. B: Condens. Matter Mater. Phys.* **2006**, *73*, 235116.
(55) Blaha, P.; Schwarz, K.; Dederichs, P. H. First-Principles Calculation of the Electric-Field Gradient in HCP Metals. *Phys. Rev. B: Condens. Matter Mater. Phys.* **1988**, *37*, 2792−2796.
(56) Schwarz, K.; Ambrosch-Draxl, C.; Blaha, P. Charge Distribution and Electric-Field Gradients in $YBa_2Cu_3O_{7-x}$. *Phys. Rev. B: Condens. Matter Mater. Phys.* **1990**, *42*, 2051−2061.
(57) Shannon, R. D. Revised Effective Ionic Radii and Systematic Studies of Interatomic Distances in Halides and Chaleogenides. *Acta Crystallogr., Sect. A: Cryst. Phys., Diffr., Theor. Gen. Crystallogr.* **1976**, *32*, 751−767.
(58) Schönberg, N. Contributions to the Knowledge of the Molybdenum-Nitrogen and the Tungsten-Nitrogen Systems. *Acta Chem. Scand.* **1954**, *8*, 204−207.
(59) Taylor, M. A.; Alonso, R. E.; Errico, L. A.; López-García, A.; de la Presa, P.; Svane, A.; Christensen, N. E. Coexistence of Different Charge States in Ta-doped Monoclinic HfO_2: Theoretical and Experimental Approaches. *Phys. Rev. B: Condens. Matter Mater. Phys.* **2010**, *82*, 165203.
(60) Assali, L. V. C.; Machado, W. V. M.; Justo, J. F. Structural and Electronic Properties of 3*d* Transition Metal Impurities in Silicon Carbide. *Phys. Rev. B: Condens. Matter Mater. Phys.* **2004**, *69*, 155212.
(61) Rentería, M.; Bibiloni, A. G.; Darriba, G. N.; Errico, L. A.; Muñoz, E. L.; Richard, D.; Runco, J. Efficiency-Optimized Low-Cost TDPAC Spectrometer Using a Versatile Routing/Coincidence Unit. *Hyperfine Interact.* **2008**, *181*, 145−155.
(62) Richard, D.; Darriba, G. N.; Errico, L. A.; Rentería, M.; Munoz, E. L. Ionic Exchange and the Local Structure in the HfO_2/Ho_2O_3 System Studied by PAC Spectroscopy. *J. Alloys Compd.* **2014**, *594*, 189−196.

DOI: 10.1021/acs.jpcc.5b11155
J. Phys. Chem. C 2016, 120, 5640−5650